Stability Analysis of Self Propelled Multi-Utility Platform for Orchard Management System using Point Manipulation Method

Ajay Kumar Roul (ajaykroul@gmail.com)
ICAR-Central Institute of agricultural Engineering
Vinod Kumar Bhargav
Central Institute of Agricultural Engineering

Original Article

Keywords: self-propelled, centre of gravity, weight moment method, point manipulation method, stability

Posted Date: July 21st, 2020

DOI: https://doi.org/10.21203/rs.3.rs-44966/v1

Stability Analysis of Self Propelled Multi-Utility Platform for Orchard Management System using Point Manipulation Method

Ajay Kumar Roul, Vinod Kumar Bhargav

ICAR-Central Institute of Agricultural Engineering, Nabibagh, Bhopal – 462038, India

Corresponding author E mail address – Ajay.Roul@icar.gov.in

Abstract

Self-propelled hydraulically operated multi-utility platform for orchard management system (SOMS) was developed to increase the accessibility of pickers to fruit on trees and to carry out orchard management practices like spraying and pruning. The platform was designed for vertical reach of 6 m and load carrying capacity of 200 kg. Point manipulation programme was developed by Microsoft Excel add in and by trial and error, position of the standard components were decided to determine the centre of gravity of the machine. Standard components were placed over the chassis in such an arrangement that, the centre of gravity (CG) always remain over the chassis during entire operation of the platform from minimum to maximum height with designed load. Forces acting on the chassis were analyzed to find out weight transfer and impending stability in various terrain conditions, various bucket positions loads on the bucket. The prediction equation for the determination of horizontal center of gravity (X_{cg}) was verified with the true value collected by keeping the wheels of SOMS on individual electronics weighing balance. The average absolute variations between the predicted and measured values of X_{cg} were within 0.44 % and 3.53%.

Key words: self-propelled, centre of gravity, weight moment method, point manipulation method, stability

1. Introduction

Fruit crops like mango, cashew, coconut, litchi and arecanut etc. are cultivated on large area in India. Harvesting, pruning and spraying of these horticultural fruit trees are difficult due to height of trees and non availability of machines. It requires fairly large numbers of seasonal labour. It is difficult to pick fruits from tall trees and usually costs more for harvesting, pruning and spraying operations. Manually operated low capacity gadgets and tree-shaking methods prevail, which are time consuming, drudgery prone, damage fruits and damage tree branches. Harvesting of fruits in India is mostly done manually by means of curved knives, pair of scissors or blades attached to a hanging basket to the distal end of bamboo sticks (Devnani, 1980) and using ladder for small height trees. Tractor three point linkage mounted elevator platform and tractor trolley mounted elevator platform or scissor lift type platforms are available in India (Kolhe and Jadhav, 2011). These types of fruit picking platforms are more stable in undulated terrain, but manoeuvrability inside the orchard is a difficult task. As orchard holdings are small in size in India, their adaptability is less because of large turning radius. Many cases canopy structure of the plant doesn't permit to move the machine easily.

In many surveys, it was reported that the catching and collecting system was effective with low damage inflicted to fruits. These harvesters allow user to reach 6 to 10 m, but turnover accidents is a major concern. French Mutualité Sociale Agricole, the second largest social security agency in France, recorded 325 accidents involving these types of machine from 2002 to 2009 and two deaths between 1995 and 2009, one following the machine's loss of stability when working on a road shoulder (Cutini et al., 2017). Stability determination is of primary importance, while designing these types of machines, looking the safety of the operator. Stability of cranes has been studied by some researchers such as Sochacki, Towarek, Klosinski and Janusz as cited by Safarzadeh et al., (2011). This paper presents a design procedure for the development of self-propelled hydraulic platform for harvesting, pruning and spraying of fruit trees considering the biological systems, engineering chassis

mechanics and its stability analysis. The major research contribution of this paper is the development of optimization tool for distribution of weights over the chassis by Microsoft Excel point manipulator tool and development of mechanics of stability analysis for design and development of any type of elevator platform for field application.

2. Hydraulic System Design

Slope and soil condition are the most critical factor for designing the self propelled picking platform. These factors directly decide the power requirements as well as stability of the machine. For stability, the center of gravity should be as close to the ground as possible while considering also the humps and bumps present in the terrain. Lugged tyre or floating tyre should be used for getting enough traction. With above assumption, a self propelled vehicle transmission system was designed. The transmission system was designed considering two conditions such as: (a) the vehicle will just climb a desired slope without slipping under design conditions (b) for vehicle starting on gradient, there should be sufficient starting torque to drive the vehicle up the gradient and this starting torque must be greater than torque required to drive the vehicle up the gradient. Total force to drive the vehicle up the gradient is the summation of force required to overcome the rolling resistance and force required to overcome gradient. The coefficients of rolling resistance (ρ) and is calculated from the equation,

$$\rho = \frac{1.2 \times W}{CI \times b \times d} + 0.04 \quad (1)$$

where, W is the total weight on the wheels, CI is cone index of the soil, b is the width of wheel, d is wheel diameter.

Assuming CI = 300 kN m^{-2} and W = 15 kN, the coefficients of rolling resistance for the orchard management system with b = 0.264 m and d = 0.78 m is 0.22. Rolling resistance for the vehicle is calculated as,

$$\mathbf{R} = \boldsymbol{\rho} \times \mathbf{W} \quad (2)$$

and the force required to overcome gradient is given by the expression,

$$\mathbf{F_g} = \mathbf{W} \times \mathbf{sin}\,\boldsymbol{\theta} \quad (3)$$

Where θ is the slope of the terrain and a maximum of 5° with the horizontal is considered for the design of the SOMS. Rolling resistance and force require to drive SOMS up the gradient is calculated as 3.18 kN and 1.28 kN, respectively and the total force required to drive the SOMS up the gradient, F is 4.46 kN. Maximum force at drive wheel before slip occurs is given by the expression,

$$\mathbf{F_s} = \boldsymbol{\mu} \times \mathbf{N} \quad (4)$$

where, μ is the coefficient of friction between the wheel and ground surface and N is the normal reaction. Considering value of μ as 0.85 and 70% of the total SOMS weight distributed over the rear traction wheel, F_s was calculated as 7.5 kN.

The wheel torque (T) is assumed equal to the total force required F_t acting at a moment arm equal to the rolling radius (r). Torque requirement was calculated for four conditions such as: (i) SOMS operating on level terrain (ii) SOMS moving up the gradient (iii) SOMS descending in gradient and (iv) SOMS starting on gradient. SOMS operating on level terrain, only rolling resistance was considered where as for the SOMS moving up the gradient, both rolling resistance and gradient force was considered. SOMS descending on the gradient, gradient will add the drive. SOMS starting on the gradient, maximum torque which can be applied at the wheel is that which will cause the wheel to slip.

Torque requirement when SOMS moving on level terrain is given by the expression,

$$\mathbf{T_l} = \mathbf{R} \times \frac{\mathbf{d}}{\mathbf{2}} \quad (5)$$

Torque requirement when SOMS moving up the gradient is given by the expression,

$$\mathbf{T_u} = (\mathbf{R} + \mathbf{F_g}) \times \frac{\mathbf{d}}{\mathbf{2}} \quad (6)$$

Torque requirement when SOMS descending on the gradient is given by the expression,

$$\mathbf{T_d} = (\mathbf{R} - \mathbf{F_g}) \times \frac{\mathbf{d}}{\mathbf{2}} \quad (7)$$

Torque requirement when SOMS starting on the gradient is given by the expression,

$$\mathbf{T_s} = \mathbf{F_s} \times \frac{\mathbf{d}}{\mathbf{2}} \quad (8)$$

Torque required for the SOMS at individual drive wheel for conditions (i), (ii), (iii) and (iv) were calculated as 603.95, 360.28, 847.62 and 1425.88 N, respectively.

Based on the maximum torque requirement, hydraulic system was designed and the circuit was developed (Fig.1). The open loop hydraulic system was adopted to power the vehicle as well as lifting and lowering the arm. Since machine was conceptualized with three wheel systems, the two wheels are required to be powered and third wheel should be caster wheel for self-steering. Hydraulic system was designed for forward and reveres movement, steering, differential action of the SOMS, raising and lowering the platform and free-wheeling the SOMS. The main part of the hydraulic system consist a fixed displacement gear pump, two fixed displacement orbital wheel motor, mobile three position four port directional control valve having centre neutral line, a double acting cylinder, double over centre valve, four port detent type directional control valve and pressure relief valve.

From the typical characteristic curves for an orbital motor, a wheel motor having displacement of 500 cm^3 per revolution could produce the maximum required torque. The actuation of the motor was done by a spring centered two bank mobile valve from the operator's platform. For lifting and lowering of platform, double acting hydraulic cylinder was used and controls for it was provided at platform as well as on the base. Mobile valves used to actuate the motors and hydraulic cylinder, were connected in parallel. Double over

centre valve was fitted across A-B line of individual motor for restricting the SOMS from over running down the slope or not allowing the SOMS to move down grade, when the system stopped on a downward slope. Two closed centre directional control valve fitted to the system for free-wheeling the motors when the SOMS is required to tow.

Flow required by the motor at maximum designed speed is given by the expression,

$$\mathbf{V} = \frac{\mathbf{D_m \times N_m}}{\mathbf{\eta_v \times 1000}} \quad (9)$$

where V is the flow rate (l min^{-1}), D_m is the motor capacity (cm^3), N_m is the rotational speed of the wheel per minute (RPM) and η_v is the volumetric efficiency of the motor.

To achieve a maximum designed speed of 3 km h^{-1}, rotational speed of wheel per minute was calculated as 20.95 and flow required by the selected motor having volumetric efficiency of 75 % was 13.97 l min^{-1}. Total flow required for both the motor was 27.94 l min^{-1}.

Form the characteristic curve of the motor, the equivalent pressure drop when the motor is on the level ground is 140 bar and it is 180 bar when the vehicle is climbing the gradient. Assuming back pressure at motor, pressure drops in the line and pressure drop across valves is approximately 4 bar each, the pressure at pump to meet maximum torque requirement is 152 bar and 192 bar, respectively when the SOMS is on level ground and the SOMS is climbing gradient.

The maximum pressure requirement is 192 bar when the SOMS is climbing the gradient and the maximum flow rate is 27.94 l min^{-1}, when the vehicle is on level ground. Speed can be reduced to 2.40 km h^{-1} on the gradient to match the equivalent power requirement in both the conditions.

Actual input power to the pump is given by the expression,

$$\mathbf{P} = \frac{\mathbf{V_m \times P_r}}{\mathbf{600 \times \eta_o}} \quad (10)$$

Where, P is the actual input power to the pump in kW, V_m is the flow rate of the pump in l min^{-1}, P_r is the pressure in bar and η_o is the overall efficiency. Using the above equation the power requirement of 7.86 kW and 7.95 kW was obtained for the operating speed of 3.0 and 2.4 km h^{-1}, respectively.

Displacement of the pump was obtained using the following equation,

$$\mathbf{D_p} = \frac{\mathbf{V_m \times 1000}}{\mathbf{N_p \times \eta_p}} \quad (11)$$

Where, D_p is the displacement of the pump per revolution in cm^3, N_p is the revolution of the pump shaft per minute and η_p is the pump volumetric efficiency. For V_m = 27.94 l min^{-1}, N_p = 2500 and η_p = 0.9; the value of D_p would be equal to 12.42.

Piston rod diameter was calculated by the expression given by Euler as,

$$\mathbf{K} = \frac{\boldsymbol{\pi^2 \times E \times J}}{\mathbf{(S \times L)^2}} \quad (12)$$

Where, K is the Buckling load in kg, E is the modulus of elasticity in kg cm^{-2}, whose value for steel is 2.1 × 10^6, J is the second moment of area of piston rod in cm^4 and L is the free equivalent buckling length in cm depending on the method of fixing the cylinder and piston rod. The cylinder is pivoted at both ends the load is fully guided.

Second moment of inertia is given by the expression,

$$\mathbf{J} = \frac{\boldsymbol{\pi \times d^4}}{\mathbf{64}} \quad (13)$$

Where, d is the diameter of rod in cm.

The lift arm is key component which carries the entire load. It is an overhanging cantilever beam. The free body shear force and bending moment diagram are shown in Fig. 2. The section dimension was determined by the expression

$$\frac{M}{\frac{(a^4-b^4)}{12}} = \frac{F}{\left(\frac{a}{2}\right)} \quad (14)$$

Where, M is the bending moment in Nm, F is the yield stress in N $m^{-2,}$ a and b is the section width of the hollow square cross section. Mild steel was chosen for the lift arm. Using the above expression and considering the standard sectional width, thickness of the section was calculated.

All other components like pins, shaft, and bushes, frame etc were designed and selected as standard/material available based on the load coming on it.

3. Modelling of the crane

CAD model of all the standard components and the chassis were developed. The external dimensions of all the components as well as their weights were measured. The position of horizontal as well as vertical center of gravity of all individual components was calculated. For very irregular structure, the centroid of the external dimension was assumed as center of gravity. Various components of SOMS, their weight and positions of horizontal center of gravity (x-distance) as well as vertical center of gravity (y-distance) of all individual components form the reference point were presented in Table 1. Center of gravity of the vehicle without boom, platform bucket and load on platform bucket was calculated by weight moment method using the equation 15 and 16.

Horizontal position of center of gravity, X_g was calculated by the expression,

$$\mathbf{X_g} = \frac{\sum(\mathbf{X}\times\mathbf{W})}{\sum \mathbf{W}} \quad (15)$$

and vertical position of center of gravity, Y_g was calculated by the expression,

$$\mathbf{Y_g} = \frac{\sum(\mathbf{Y}\times\mathbf{W})}{\sum \mathbf{W}} \quad (16)$$

The horizontal center of gravity of SOMS was calculated by using the following expression:

$$X_{cg} = \frac{(\sum(\sum X_1 \times W_1 + X_2 \times W_2 + X_b \times W_b)}{\sum(W_1 + W_2 + W_b)} \quad (17)$$

Where, W_1 = weight of SOMS without boom and bucket, W_2 = weight of boom, W_b = weight of platform bucket, X_2 = position of center of gravity of boom, X_b= position of center of gravity of platform bucket

Point manipulation programme was developed by Microsoft Excel add in (Fig. 3) and by trial and error, position of the standard components were determined. Standard components were placed over the chassis to distribute 70 and 30% static load over the front wheel and rear wheel, respectively.

Weight distribution and position of centre of gravity found from the above analysis at zero fruit load condition standing on the level ground is summarized in Table 2.

The concept was translated in solid model using CAD software PTC Creo element 1 (Fig. 4)

Aanalysis were per-formed based on maximum weight of various components as well as forces and moments acting on those components (Segerlind, 2010). The allowable stress method based on IS/ISO 8686 standard 2006 was used to assess the strength of the components. Brief specification of the developed SOMS is presented in the Table 3.

4. Stability analyses

As the vehicle is designed for the field application, it has to ride over very rough terrain. Safety of the operator should be the primary issue, while designing this type platform. Stability calculation must be done before being used for the field application. The complete process includes the proper selection of shape and dimensions, weight distribution etc.

Position of centre of gravity plays an important role in deciding the stability of the platform. Point of center of gravity is a descriptive one. Its location changes as the balance of weight at the platform changes. For example (a) when the vehicle is still, the center of gravity is at

original position (b) when an operator board the platform and add his weight, the center of gravity moves immediately from original point forward to a new point where the sum of weights is balanced (c) When the operator pick the fruit and add the weight of the fruit to the picking container, the point of center of gravity continues to move according to the added weight and (d) when the arm lifted, the center of gravity moves up and backward since the tower's leverage shortens**.**

The vehicle is supported by the ground, with its three wheels, and creates a triangle. As long as the line of center of gravity remains in the area of the triangle, the machine will be stable. If the line of the center of gravity goes beyond the area of the triangle, the machine will turn over in the same direction. The lower the point of the center of gravity (i.e., closer to the ground), the greater may be the slope before the line of the center of gravity will go outside the area of the triangle.

4.1. Static and dynamic analysis of the longitudinal stability

Longitudinal stability was analysed for the SOMS while it moves on both the upward slope and downward slope with carrying maximum pay load at the bucket and at various height of the elevator bucket. Free body diagram for static and dynamic model with application of forces were developed and presented in Fig. 5. Stability of the SOMS was checked up to 6° longitudinal slope.

Using D' Alembert's principle, reaction forces acting at the ground wheels in static as well as dynamic condition and shifting of position centre of gravity on longitudinal slopes are obtained by the following equations:

Case I: When SOMS is travelling on upward longitudinal slopes, the static reaction forces are:

$$W'_f = \left(W \times \cos\alpha \times \frac{X_r}{X}\right) - \left(W \times \sin\alpha \times \frac{Y_g}{X}\right) \quad (18)$$

$$W'_r = W \times \cos\alpha - W'_f \quad (19)$$

and the dynamic reaction forces are:

$$R_{Rear} = W'_r + \left(W \times \sin\alpha \times \frac{R_r + Y_g}{X}\right) \quad (20)$$

$$R_{Front} = W'_f - \left(W \times \sin\alpha \times \frac{R_r + Y_g}{X}\right) \quad (21)$$

Case II: When SOMS is travelling on downward longitudinal slopes, the static reaction forces are:

$$W'_r = \left(W \times \cos\alpha \times \frac{X_f}{X}\right) - \left(W \times \sin\alpha \times \frac{Y_g}{X}\right) \quad (22)$$

$$W'_f = W \times \cos\alpha - W'_r \quad (23)$$

and the dynamic reaction forces are:

$$R_{Rear} = W'_r - \left(W \times \sin\alpha \times \frac{R_r + Y_g}{X}\right) \quad (24)$$

$$R_{Front} = W'_f + \left(W \times \sin\alpha \times \frac{R_r + Y_g}{X}\right) \quad (25)$$

4.2. Static and dynamic analysis of the lateral stability

Lateral stability of the SOMS in static and dynamic condition was analysed for the slope of the surface up to 6° and taking moment about right front wheels. SOMS will be overturned when the magnitude of reaction forces at the left front wheel will be zero and vice versa or the projected line of centre of gravity will fall beyond the outside area of the triangle. Free body diagram for static and dynamic model with application of forces were developed and presented in Fig. 6.

When SOMS travelling on lateral slopes, the static reaction forces are:

$$W'_L = \left(W \times \cos\alpha \times \frac{Z - X_L}{Z}\right) - \left(W \times \sin\alpha \times \frac{Y_g}{Z}\right) \quad (26)$$

$$W'_R = W \times \cos\alpha - W'_L \quad (27)$$

and the dynamic reaction forces are:

$$R_{Left} = W'_L + \left(\frac{m \times u^2}{R} \times \sin\alpha \times \frac{X_r}{Z}\right) + \left(\frac{Y_g}{Z} \times \frac{m \times u^2}{R} \times \cos\alpha - W \times \sin\alpha\right) \quad (28)$$

$$R_{Right} = W'_R + \left(\frac{m \times u^2}{R} \times \sin\alpha \times \frac{X_r}{Z}\right) + \left(\frac{Y_g}{Z} \times W \times \sin\alpha - \frac{m \times u^2}{R} \times \cos\alpha\right) \quad (29)$$

5. Results and discussion

Using the Eq. 18 to 29 for the stability calculation, wheel reaction forces are calculated for no fruit load, 100, 150 and 200 kg fruit load at six vertical positions of the lift arm such as at the original position of the lift arm, lift arm parallel to the horizontal, 10°, 20°, 35°, 45° and 60° with respect to horizontal in anticlockwise direction. Wheel reaction forces with various loads and vertical positions of the lift arm was calculated for every degree rise of the longitudinal as well as lateral slope up to 6°. As explained earlier reaction force at the rear wheel is the critical factor, when the bucket is fully loaded and the lift arm is at its lowest position. But for the lift arms at its highest position, both the wheel reactions are important. Results of static conditions are summarized in the Table 4.

Results indicate that the SOMS is stable within the designed condition with minimum of wheel reaction force of 11.5, 10.13 and 41.87 % existing on longitudinal upward slope, longitudinal downward slope and lateral slope, respectively. In the analysis, it was also found that three is not much variation between the static and dynamic condition and the variations are in the order of one to two percent.

Displacement of horizontal position of centre of gravity (X_{cg}) and vertical position of centre of gravity (Y_{cg}) with various fruit loads and vertical positions of the lift arm was calculated for different slope of the field using Eq. 17 to 28. Rear wheel ground contact point was considered as reference point. Figure 7 represents the displacement of the positions of the X_{cg}

and Y_{cg} with increase in fruit load at the bucket in the levelled ground, 6° upward and downward longitudinal slope and 6° lateral slope. It can be seen from the Fig. 7 that, with increase in upward slope, the position of X_{cg} shifting towards the rear wheel whereas it is shifting away from the rear wheel for the downward slope. With increase in vertical position of the bucket, the position of X_{cg} shifting towards the rear wheel for both the upward and downward slope, resulting in increasing stability of the SOMS.

At 6° lateral slope, the position of Y_{cg} is shifting 165 mm to either side of the centre line of the SOMS. The projected line of the centre of gravity passing a point just 201.3 mm away from the centre line and is well within the area of triangle created by the three wheels of the SOMS. The designed vehicle could be operated in more than 6° lateral slope, as it is found from the results of the analysis, but it is recommended only up to 6° considering the condition of the field where both longitudinal and lateral slope may exists.

5.1 Validation of the predicted center of gravity with measured value

The prediction equation developed for the determination of X_{cg} was verified with the true value collected through laboratory experiments. The wheels of the SOMS were placed over three independent electronics weighing balance (Fig. 8). Various loads were placed on the bucket of SOMS and reaction loads at individual wheel were observed through weighing balance. To simulate the various terrain conditions, wheels are lifted by to the desired height e.g. for longitudinal upward slope, the two front wheels are lifted to desired height keeping the rear wheel on original level. Then the bucket of the SOMS was lifted to various reach height and weights at the weighing balances were recorded. Knowing the wheel reactions and the distance between wheel centres, the X_{cg} was calculated.

The comparison of measured and predicted values of the X_{cg} w.r.t to the height of the bucket of SOMS for all terrain conditions and two extreme loading conditions (no load and

maximum design load) are plotted in Fig. 9. A close relationship was found between the measured and predicted value of X_{cg}. For lateral slope, the developed equation under predicted whereas for all other three terrain conditions it was over predicted. The measured and predicted values of the X_{cg} for all terrain conditions are plotted in Fig. 10 and results of statistical analysis for model validation are given in Table 5. The percentage variation of the predicted values for level ground, upward slope, downward slope and lateral slope were found to be 0.72 to 3.40, 0.84 to 2.43, 0.44 to 1.91 and -1.91 to -3.53, respectively.

A close agreement between observed and predicted values of the X_{cg} was found with slope varied from 0.98 to 1.00 and coefficient of determination varied from 0.87 to 1.08 for all terrain and loading conditions. These variations are considered acceptable considering the variations existed in assumed center of gravity and actual center of gravity of all the components of the SOMS, slight variation in model weight and measured weight and changes in shape of the hydraulic oil in the reservoir as well as water in the spraying tank in tilted condition of the SOMS.

6. Conclusions

This paper presents a innovative method to optimize the weight distribution over a chassis for designing a self-propelled elevator lift by using Microsoft Excel point manipulator add in tool. The position of Centre of gravity in any plane and weight distribution over the ground supported wheel can easily be determined by simply scrolling the horizontal and vertical scrollbar. The design process essentially concentrated on the design of hydrostatic transmission for a self propelled machine, design of hydraulic systems for other functions and development of mechanics for analysis of stability to design of a self propelled elevator lift with the aim to decrease the hazards associated with field application. This not only helps the operator for safe operation but also future industry for development of these types of elevator lift.

7. Declaration

7.1 Availability of data and materials

The datasets used and/or analysed during the current study are available from the corresponding author on reasonable request.

7.2 Competing interests

The authors declare that they have no competing interests" in this section.

7.3 Funding

Not applicable

7.4 Authors' contributions

All authors read and approved the final manuscript**.**

7.5 Acknowledgements

Not applicable

7. References

Safarzadeh, D., Sulaiman, S., Aziz, F. A., Ahmad, D. B. & Majzoobi, G. H. (2011). The design process of a self-propelled floor crane. Journal of Terramechanics, 48 (2), 157–168.

Devnani, R.S. (1980). Harvesting Equipment Developed in India, Technical bulletin, ICAR-Central Institute of Agricultural Engineering.

IS/ISO 8686-1: Part-1, (1989). Cranes - Design principle for loads and load combinations.

Kolhe, K.P., & Jadhav B.B. (2011). Testing and performance evaluation of tractor mounted hydraulic elevator for mango orchard. American Journal of Engineering. and Applied . Science, 4 (1), 179-186.

346 Liljedahl, j. B., Turnquiest, P. K., Smith, D. W., & Hoki, M. (2004). Tractors and their
347 power units. (4th Ed.). New York: Wiley & Sons, (Chapter 11).

348 Macmillan, R.H. (2002). The Mechanics of Tractor - Implement Performance: Theory and
349 Worked Examples, (Chapter 6). Printed from: http://www.eprints.unimelb.edu.au.

350 Cutini, M., Brambilla, M., Bisaglia, C., Melzi, S., Sabbioni, E., Vignati, M., Cavallo, E., &
351 Laurendi, V. (2017). A study of the lateral stability of self-propelled fruit harvesters.
352 Agriculture, 7 (11), 92; doi:10.3390/agriculture7110092.

353 Segerlind, L.J. (2010). Design of a floor crane, Designing structural components for
354 machine. St. Joseph, Michigan: ASABE, (Chapter 13).

355 **Manuscript**

α = angle of slope
α_s = Tip angle of tractor rigid body @ ground contact point under static condition
ρ = coefficient of rolling resistance
g = centre of gravity of earth
H_P = height of platform base from ground
m = total mass of the SOMS
R = turning radius of SOMS
R_f = radius of front wheel
R_r= radius of rear wheel
u = forward velocity of SOMS
W = weight of SOMS
W_f = weight at front wheel
W'_f = weight at front wheel on slope
W_r = weight at rear wheel
X = wheel base
X" = wheel base at raised condition
X_{cg} = Distance between Rear Wheel to CG from front view
X_f = distance between front wheel to CG
X'_f = distance between front wheel to CG at slope
X_{fw} = Distance between Front Wheel to CG from front view

X_r = distance between rear wheel to CG

X'_r = distance between rear wheel to CG at slope

Y' = height from base to centre of front wheel

Y = height from base to front wheel

Y_1 = height from CG @ horizontal condition to CG @ slope condition

Y_{cg} = total height of centre of gravity at slope condition from ground @ horizontal level

Y_g = CG height from centre of rear wheel at horizontal level

Y'_g = height CG from ground surface at horizontal level

Z = track width

α_s = Tip angle of tractor rigid body @ ground contact point under static condition

Figures

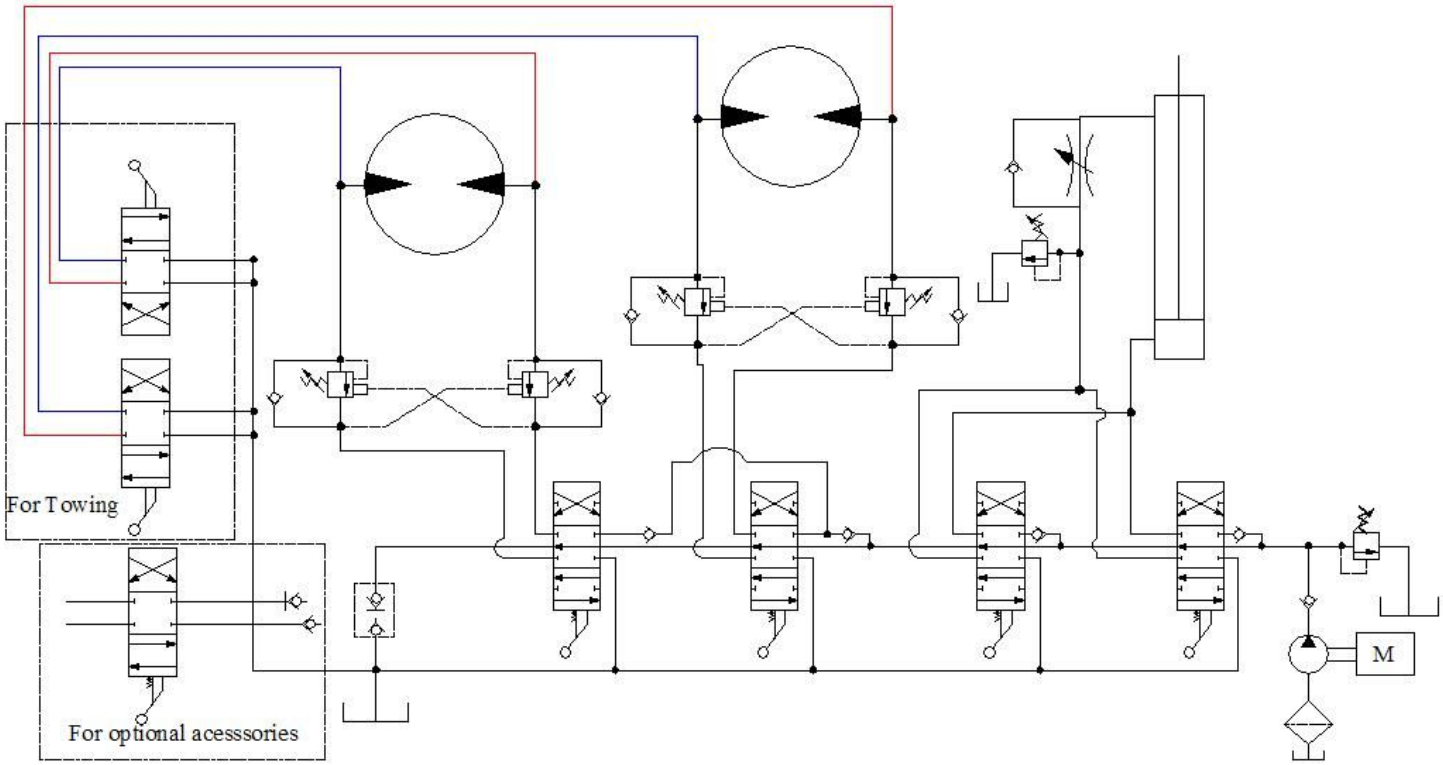

Figure 1

Hydraulic circuit diagram of SOMS.

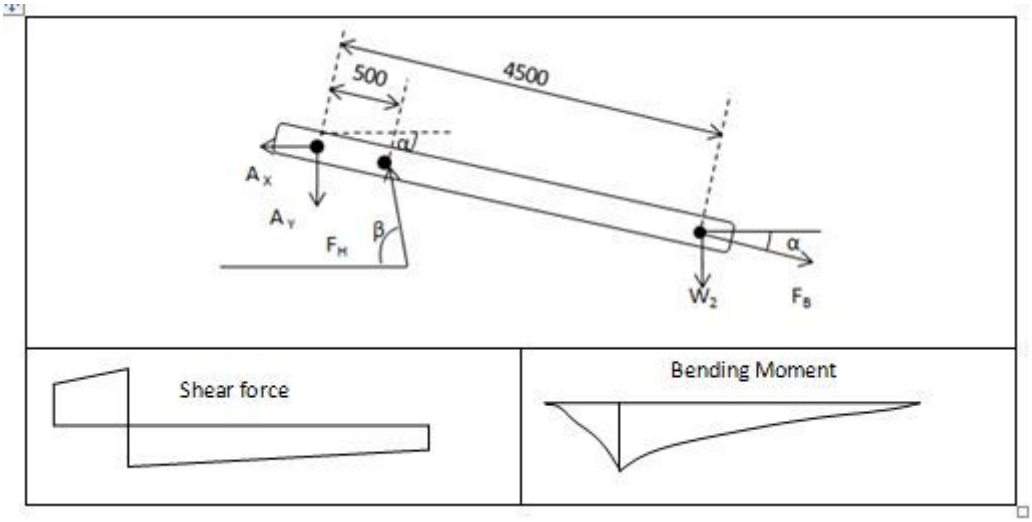

Figure 2

Free body, shear force and bending moment diagram.

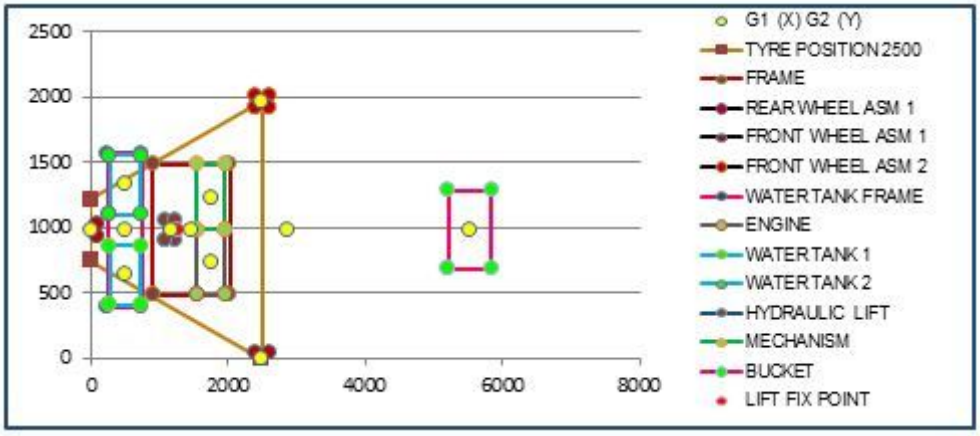

Figure 3

Point manipulation method to optimize the center of gravity.

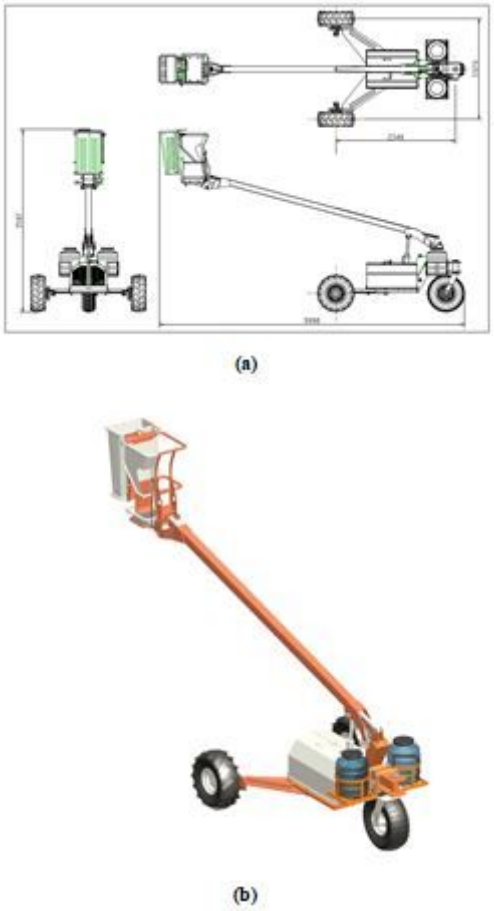

Figure 4

Computer models of the SOMS: (a) wire frame and (b) solid 3 D model.

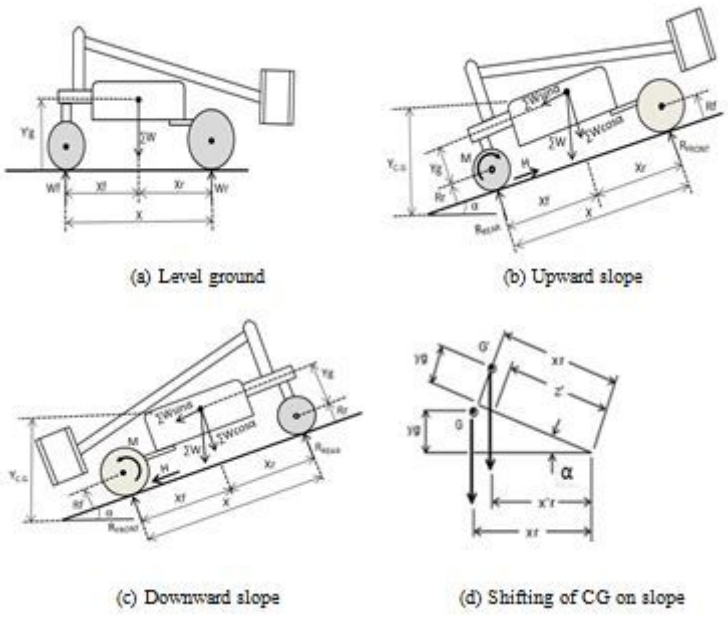

Figure 5

Free body diagram of the static and dynamic model of longitudinal stability in (a) Level ground (b) Upward slope (c) Downward slope (D) Shifting of CG on slope.

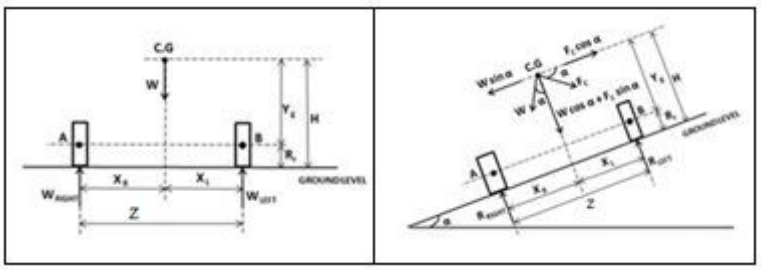

Figure 6

Free body diagram of the static and dynamic model of the lateral stability.

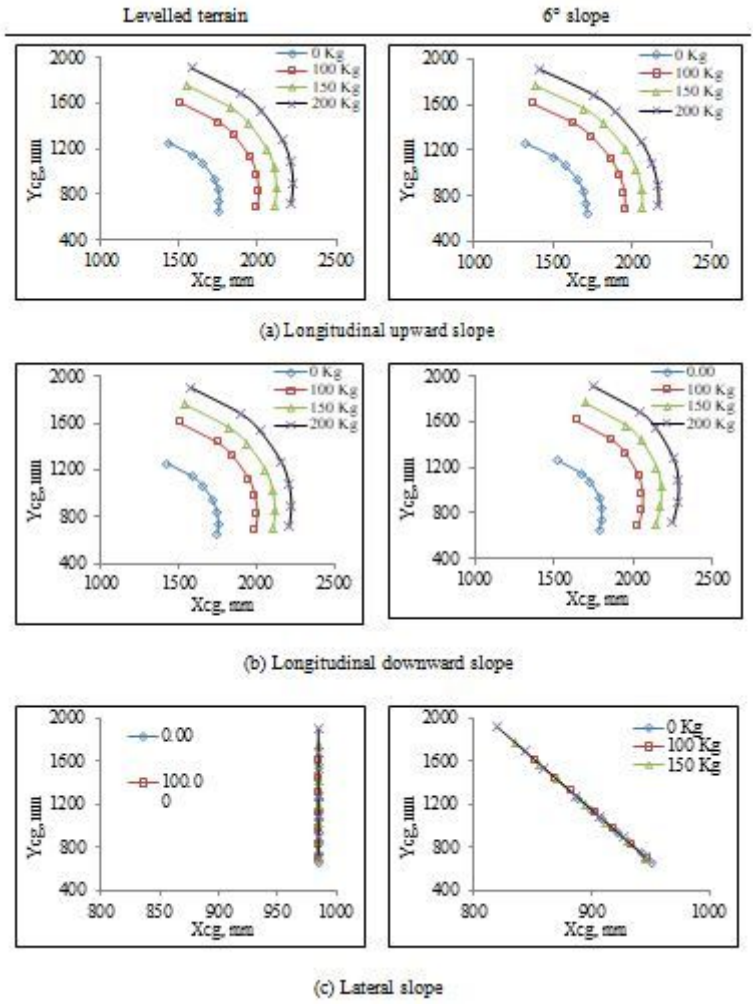

Figure 7

Displacement of positions of Xcg and Ycg with fruit load and degree of slope in (a) Levelled terrain (b) Longitudinal upward 6°slope (c) Longitudinal downward 6°slope (d) lateral 6°slope.

Figure 8

Experimental setup to measure Xcg.

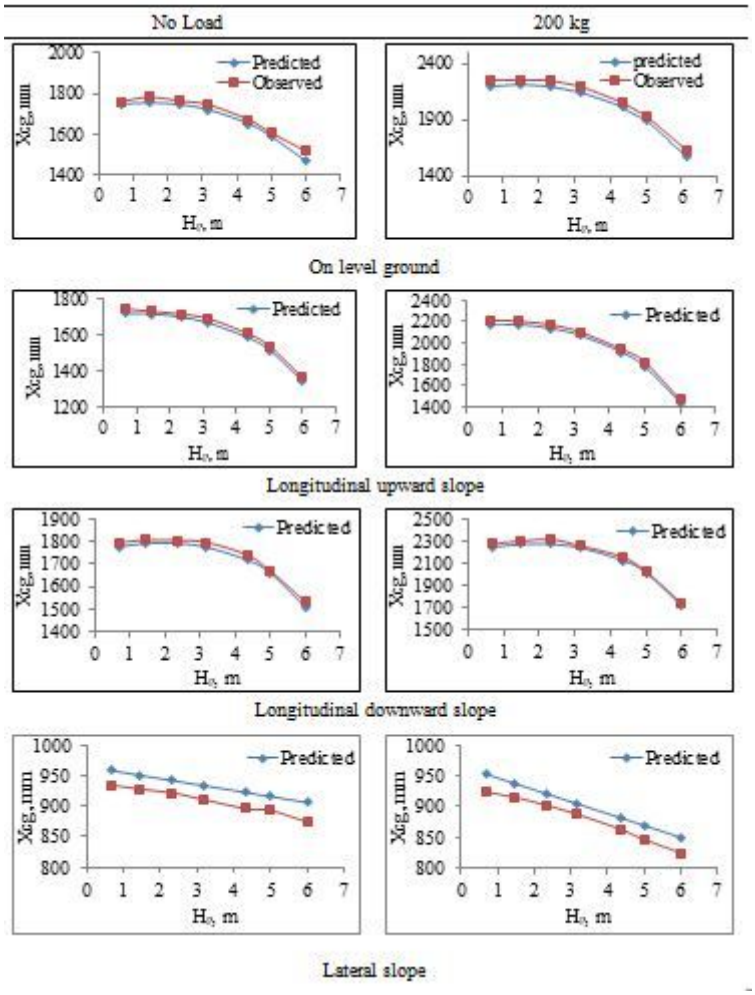

Figure 9

Comparison of measured and predicted values of the Xcg w.r.t to the height of the bucket on (a) level ground (b) Longitudinal upward slope (c) Longitudinal downward slope (d) Lateral slope.

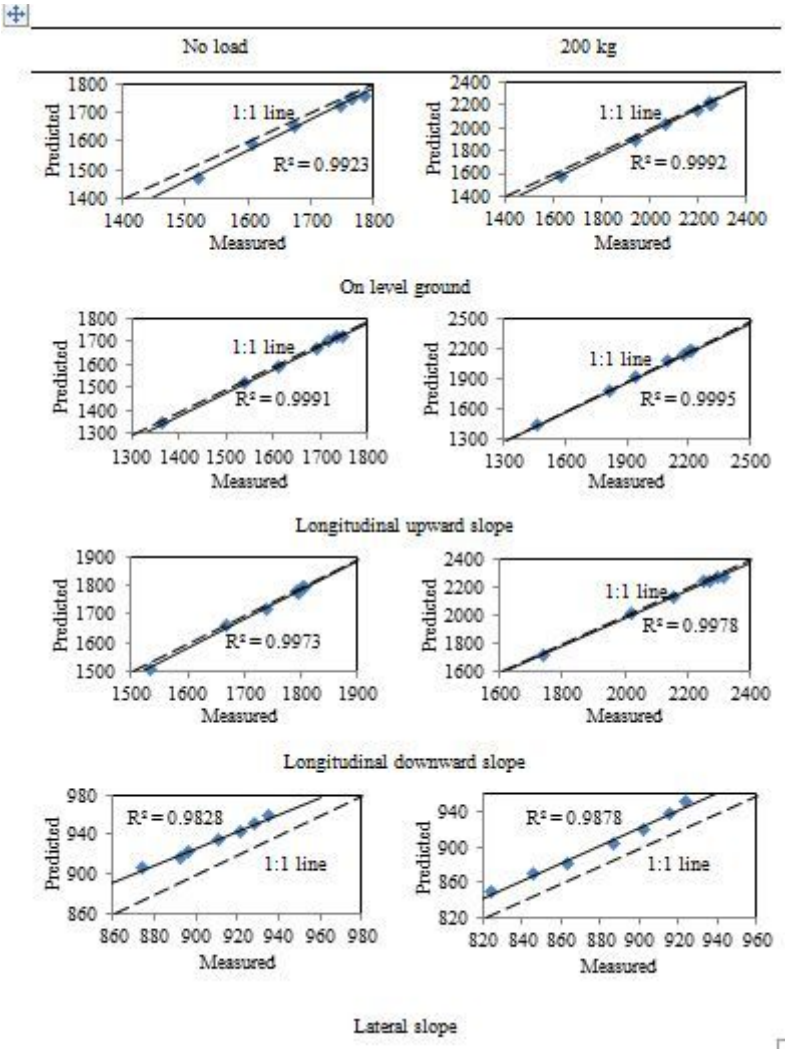

Figure 10

Validation of the measured and predicated values of Xcg on (a) level ground (b) Longitudinal upward slope (c) Longitudinal downward slope (d) Lateral slope.